Materials Today Physics 38 (2023) 101248

Contents lists available at ScienceDirect

Materials Today Physics

journal homepage: www.journals.elsevier.com/materials-today-physics

High-capacity hydrogen storage through molecularly restructured and confined hydrogen hydrates

Rojan Firuznia [a], Amir Abutalib [b,c], Alireza Hakimian [a], Sina Nazifi [a], Zixu Huang [a], T. Randall Lee [c,d], Jeffrey D. Rimer [b,c], Hadi Ghasemi [a,b,*]

[a] Department of Mechanical Engineering, University of Houston, 4226 Martin Luther King Blvd, Houston, TX, 77204, USA
[b] Department of Chemical and Biomolecular Engineering, University of Houston, 4226 Martin Luther King Blvd. Houston, Texas, 77204, USA
[c] Department of Chemistry, University of Houston, 3585 Cullen Blvd., Room 112, Houston, TX, 77204, USA
[d] Texas Center for Superconductivity, University of Houston, 3369 Cullen Blvd., Suite 202, Houston, TX, 77204, USA

ARTICLE INFO

Keywords:
Hydrogen
Storage
Nanoconfinements
Mesoporous zeolite
Hydrates

ABSTRACT

In the future landscape of sustainable energies and in combating global climate challenges, hydrogen plays a crucial role in both stationary and portable energy systems that currently supply 18 % of the total energy demand. High-capacity, safe, and cost-effective hydrogen storage is critical for advancing the hydrogen economy but remains a dauting challenge. A range of advanced material systems including metal hydrides, metal-organic frameworks, and 2D materials have been explored in efforts to achieve high storage capacity, but high operating pressures, low charging/discharging rates, and energy intensive discharging processes have hindered their development and deployment. Here, we report a green material paradigm for high storage capacity with fast charging/discharging and ambient temperature discharging. The material platform is a modified zeolite with rationally tuned pores and modified surface chemistry that exhibits long-term stability and stores hydrogen gas in the form of hydrogen hydrates. The selected pore dimensions enhance the hydrogen solubility through restructuring of water molecules, and the surface chemistry of the material leads to enhanced double donor-acceptor bonds with water molecules for enhanced hydrogen storage capacity. The material enables hydrogen storage in hydrogen hydrate form at 8–10 bar dropping the required storage pressure by two orders of magnitude lower compared to state-of-the-art materials and addresses long-standing hurdles of high operating pressure and slow formation kinetics of hydrogen hydrates providing a promising platform for hydrogen storage.

1. Introduction

Global energy demand has seen a substantial increase in the past decade, from 408 EJ in 2000 to 585 EJ in 2019 [1], fueled by the world's population growth and advanced technologies. As fossil fuels are the main source to fulfill this demand, global concerns on climate change and air and water pollution are mounting [2]. Hydrogen (H_2) is one of the most suitable options among all the sustainable sources [3] to address these concerns as it has one of the highest energy contents per unit mass (142 MJ/kg) compared with all other fuels [4], and the only product of H_2 combustion is water vapor, which makes it a zero-emission fuel. Projections indicate that H_2 will provide 18 % of the total global energy demand by 2050 [5]. This transition, however, requires these prerequisites to be fulfilled: identifying suitable H_2 production sources and optimizing H_2 production techniques and storage methods. Among these, H_2 storage is a key enabling technology for the deployment of H_2 in applications including stationary power, portable power, and transportation. Besides the high storage capacity, the storage systems must have both acceptable operating temperatures and pressures, fast charging and discharging rates, and minimal energy required for the discharging process [6,7].

A range of materials have been explored for H_2 storage including porous materials [8,9], metal hydrides [10–12], 2D materials [13,14] and others [15]. Porous media store H_2 through physisorption/chemisorption on inner surfaces of the pores. Blankenship et al. [16] reported a storage capacity of 8.1 wt% in oxygen-rich activated carbons at 77 K and 20 bar, but the capacity drops to 1.2 wt% at room temperature and 30 bar. Low silica type X zeolites reported by Li et al. [17] achieved a storage capacity of 1.5 wt% at 77 K and 1 bar. Metal hydrides are a class of materials containing metal or metalloid

* Corresponding author. Department of Mechanical Engineering and Department of Chemical and Biomolecular Engineering, University of Houston, USA.
E-mail address: hghasemi@uh.edu (H. Ghasemi).

https://doi.org/10.1016/j.mtphys.2023.101248
Received 28 August 2023; Received in revised form 3 October 2023; Accepted 3 October 2023
Available online 4 October 2023

bonded to hydrogen and are classified based on the nature of the chemical bonding (ionic, metallic, or covalent). Borzone et al. [18] showed that the Intermetallic hydride $LaNi_{4.5}Sn_{0.5}$ can reach a storage capacity of 1 wt% at a pressure of 10 bar and a temperature of 298 K. Another study by Choudhari et al. [19] has demonstrated that $NaAlH_4$ has a storage capacity of 3.7 wt% at 132 °C and 1 bar pressure. Although reasonable gravimetric storage capacities can be achieved through metal hydrides, there is a need to enhance the kinetics for the charging and discharging processes. In addition, the H_2 discharging process requires either vacuum conditions or high temperatures. On 2D materials from incompletely etched Ti_2CT_x, Liu et al. [20] were able to reach a high storage capacity of 8.8 wt% at ambient temperature and 60 bar while the discharging process required an increased temperature to 370 K. Separately, Li et al. [15] introduced Pd nanocrystals covered by the metal-organic framework (MOF) HKUST-1 for H_2 storage, which have twice the storage capacity of bare Pd nanocrystals. These covered nanocrystals offer a storage capacity of 0.87 H per Pd atom at 303 K and 1 bar. Recently, Farrando-Perez et al. [21] showed that through confined activated carbon structures, hydrogen hydrate could form at 30 % lower pressure (~1000 bar) compared to bulk water with fast kinetics and conversion. This reduction in formation pressure was attributed to a confinement effect within the inner cavities of carbons. Despite these progresses in materials design, identifying materials with high storage capacities at low operating pressures accompanied by high charging and discharging rates without the prerequisite of high temperatures for discharging remains a challenge.

Here, we report a paradigm in the development of sustainable materials for hydrogen storage in the form of hydrogen hydrates at low operating pressure (10 bar) with unprecedented fast charging/discharging rates and discharging at ambient temperature. Hydrogen hydrate functions based on trapping H_2 molecules in the lattices structure of host molecules (i.e., water). In comparison with the other methods, hydrogen storage through hydrates has promising advantages including ambient condition discharging, low-cost material, operational safety, and no negative environmental impacts (e.g., no generated pollutant/toxic substances) [22]. Despite these promising features of hydrogen hydrates, the required high storage pressures and/or low storage temperatures, low storage capacities, and slow charging rates have hindered their commercial deployment until now. Through a rationally designed morphological and functional material platform, we boosted the storage capacity of hydrates by 200 times and the formation rate by 10 times compare to bulk water and THF [23,24]. The US Department of Energy (DOE) target for 2025 for onboard light-duty vehicles, material-handling equipment, and portable power applications are 5.5 % gravimetric storage capacity and 0.04 (kg H_2/L system) volumetric storage capacity in the working pressure range of 5–12 bar with working temperature range of −40 to 85 °C [25]. Herein we refer to this hierarchical FAU-type zeolite as Z3. While Z3 material promises outstanding storage capacity in the target pressure and temperature range by DOE, its gravimetric storage capacity and volumetric density needs further push to meet all the metrics in DOE 2025 target.

The storage of H_2 molecules in hydrate structures occurs through physical entrapment of H_2 molecules in water cages as opposed to a chemical reaction. The mechanism is primarily governed by van der Waals (dispersion) forces, intermolecular interactions, and hydrogen bonding, where the strong hydrogen bonds hold the host framework together. Phase diagrams of water-hydrogen at a temperature range of 200–330 K and pressures up to 2.5 GPa show various forms of hydrogen hydrates including classical clathrate hydrates with cubic structure II (sII) (unit cell of 136 water molecules + different numbers of hydrogen molecules in large and small cavities), hydrogen-filled ice I_h (unit cell of 64 water molecules with maximum $32H_2$ molecules), hydrogen-filled ice II (C1 phase, unit cell of 288 water molecules with maximum $48H_2$ molecules), and hydrogen-filled ice Ic (C2 phase, unit cell of 64 water molecules and $64H_2$ molecules) [26,27]. In addition, it has been shown that H_2 could be incorporated in a hydrate with cubic structure (I) [28] (contains two pentagonal dodecahedron (5^{12}) cages and six tetrakaidecahedron ($5^{12}6^2$) cages) and hexagonal hydrate structure H (sH) [29] (three pentagonal dodecahedron (5^{12}) cages, two irregular dodecahedron ($4^35,^66^3$) cages, and one icosahedron ($5^{12}6^8$) cage). Each water cage of the host structure usually contains one gas molecule; however, for small molecules like H_2, multiple occupancy is possible. Mostly, the storage of H_2 in hydrate structures happens at high pressures (e.g., 200 MPa at 273 K) [30] or low temperatures (e.g., 0.1 MPa at 100K). It has been shown that second guest molecules, referred to as promoters, can facilitate hydrate formation at the expense of lower hydrogen storage capacity. For example, Lee et al. [24] decreased the required pressure for H_2 storage from 200 MPa to 12 MPa by filling the larger cavity (hydrate cages) with tetrahydrofuran (THF) to stabilize the hydrate structure. Through studies of various promoters, it was found that THF is the most efficient second guest molecules for hydrate formation [31]. Frankcombe et al. [32] performed molecular dynamics (MD) simulations of H_2-containing type-sII hydrate and found two different levels of H_2 mobility. Although no migration of H_2 was observed in small cages, H_2 was remarkably mobile in large cages, which can lead to migration of the H_2 out of the hydrate phase into the gas phase. The presence of promoter molecules, such as THF, leads to their occupation of large cages, which can block H_2 migration paths. The H_2 contained within the large cages would thus maintain "mechanical" resistance against hydrate cage collapse, which demonstrates the stabilizing effect of promoters.

In this work, rather than stabilize hydrate formation through a mixture of water, H_2 gas, and second guest molecules, we introduce a host framework material for hydrogen hydrate formation. The framework material has five distinct features: (1) It provides a platform for interfacial hydrate formation rather than bulk hydrate formation; (2) Through rational selection of pore dimensions, the water molecules are layered in the pore of the host material leading to 2–3 times enhanced hydrogen absorption; (3) The curvature of the pores in the host framework enhances the nucleation rate of hydrate particles; and (4) The chemistry of pore surface allows for restructuring of water molecules at the interface leading to the formation of DDAA (double donor-double acceptor bonds) and consequently a high nucleation rate and high hydrogen storage capacity, demonstrated by FTIR spectroscopy. The host material is schematically shown in Fig. 1a which is a powder form of zeolite Y synthesized with a pore size of 2.4 nm and a surface area of 1100 m^2g^{-1} using a process developed by Garcia-Martinez and coworkers [33,34]that offers controlled mesoporosity. The procedure for the development of Z3 is provided as Supplementary Materials, S1. The pores are filled with a solution of THF and water with 10 mol% THF concentration. Compared to slow diffusion of hydrogen gas in bulk water for bulk hydrate formation, this structure directs the hydrate formation to confined water in the pores. Furthermore, the aluminosilicate framework of Z3 provides a 3D configuration for hydrogen-gas water interaction rather than the 2D planar interface of water-H_2 in a bulk hydrate formation configuration. We examined hydrogen solubility in various pore sizes of a representative zeolite sample (zeolite 13X) through the experimental procedure discussed in Supplementary Materials, S2. The optimal pore size was found to be 2–3 nm for maximum hydrogen solubility as shown in Fig. 1b. In FAU-type zeolite with this pore diameter, the water molecules form an ordered ice-like structure in the pores, which confines gas molecules in the regions of low water density and leads to an approximate 2-fold enhancement of hydrogen solubility in the structured water. Even though gas solubility enhancement is observed in pores a few nm in size, the solubility in 1 nm pores is lower because the high curvature of the surface prevents water from strongly ordering. Conversely, gas solubility in 10 nm pores is almost similar to that in the bulk liquid [35,36]. For a pore filled with water/THF, hydrogen hydrate nuclei are formed on a concave surface. The high concavity of the zeolite pore walls leads to a drastic drop in the Gibbs energy barrier ($\Delta G^* = \Delta G_{hom} f(m,x)$) for hydrate nucleation through the shape function $f(m,x)$ [37], Fig. 1c. It is noted that the

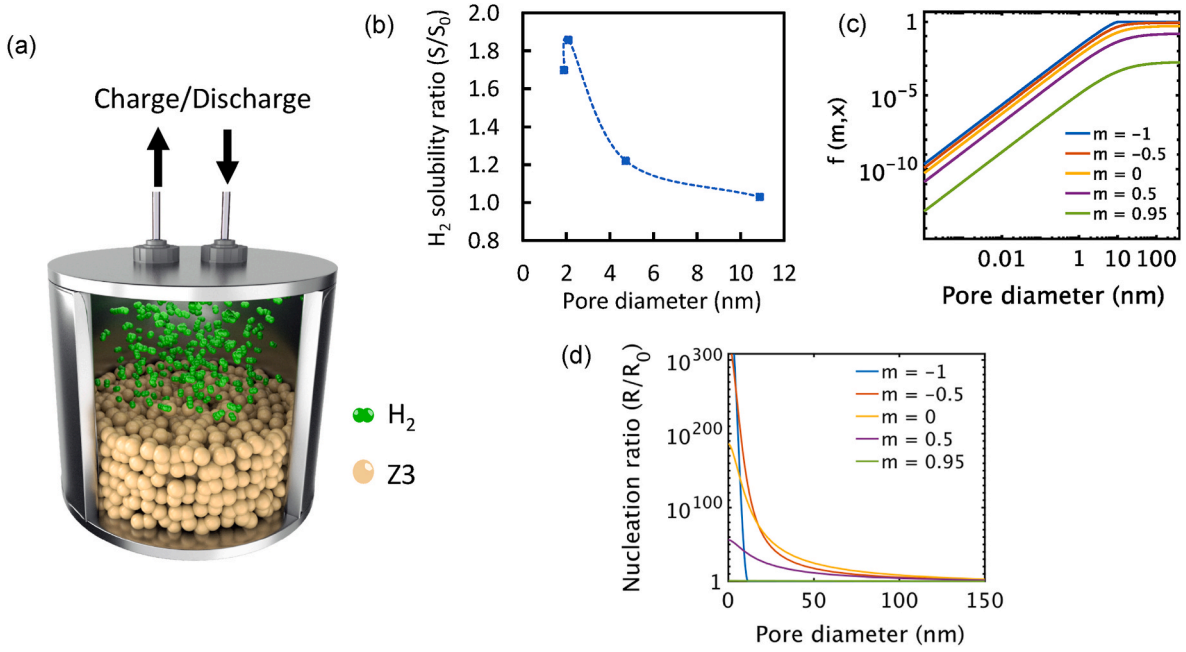

Fig. 1. **(a)** Schematic of a material platform for high-capacity hydrogen storage in which a powder of mesoporous zeolite Z3 with a pore diameter of 2.4 nm is placed at the bottom of the chamber. Hydrogen gas (green) is stored in the form of hydrogen hydrate in the Z3 pores. **(b)** The role of zeolite (FAU type) pore diameter on hydrogen solubility compared to the bulk material. The ordering of water molecules in pores spanning 2–3 nm leads to approximately 2-fold enhancement of hydrogen solubility. **(c)** The role of concavity of pores with dimensions much smaller than critical nucleus size (~6.82 nm) on shape function. A reduced value of *f(m, x)* corresponds to a lower Gibbs energy barrier for hydrate nucleation. **(d)** The role of pore size on the nucleation rate of hydrogen hydrates compared to the bulk medium. (For interpretation of the references to colour in this figure legend, the reader is referred to the Web version of this article.)

concavity affects the value of x in this function, Supplementary Materials, S3. Consequently, the reduced shape function and concomitantly the reduced Gibbs energy barrier leads to significant enhancement in the hydrogen hydrate nucleation rate, as shown in Fig. 1d.

1.1. Experimental procedure for hydrogen storage

The required concentration of water/THF solution (10 mol% THF) was prepared by adding a known quantity of THF in deionized (DI) water. To maintain homogeneity of the prepared solution, it was mixed using a magnetic stirrer for approximately 5 min. For the case of hydrate formation with a material platform, we injected a specific quantity of water/THF solution (10 mol% THF) into the pores of Z3 in proportion to the total volume of its pores. The BET result indicates the pore volume of 0.677047 cm^3/g. By adjusting the solution quantity based on the calculated pore volume, we ensured accurate and proportional injection into the Z3. Once it became completely wet, we placed the sample inside the chamber and connected it to the circulating cooling jacket. The vacuum pump was then turned on to achieve almost vacuum condition (~50 Pa) inside the chamber. The vacuum step only lasted for 20s. At the given temperature, the water vapor pressure is estimated to be around 0.24 psi, indicating a relatively low value. Utilizing the ideal gas equation and considering the vessel volume, it is possible to compute that any potential water loss is expected to be below 0.01 g. No change in the temperature of the vessel was observed suggesting no meaningful evaporation. To ensure elimination of any air bubbles in the chamber, it was pressurized with gas to approximately 0.5 MPa and depressurized to atmospheric pressure three times. The cooling temperature was then set at 263 K and once reaching steady state, was introduced into the chamber and pressurized to 10 bar. The experiment consists of two steps. In the first step, we saturate water and THF with hydrogen prior to the initiation of hydrate formation. After approximately 20 min of the process, the pressure curve stabilizes, indicating that the water and THF are fully saturated with hydrogen. Then, we proceed to the hydrate formation step. Here, we initiate hydrate formation by reducing the temperature and monitoring the point at which hydrate formation starts. This leads to an exothermic reaction that increases the system temperature. The two-step experiment design serves two main purposes: firstly, to achieve water saturation before hydrate formation, and secondly, to determine the temperature at which hydrate formation is initiated. This approach simplifies the analysis as hydrogen absorption in water and hydrate formation do not occur simultaneously. We extended the experiment duration to ensure hydrate formation completion. It can be assumed that this was a quasi-isobaric experiment since the pressure drop during the experiment is less than 1 bar as a result of gas consumption. During H_2 diffusion and the induction time, the system remains isothermal; however, owing to the exothermicity of hydrogen hydrate formation, the temperature of the system rises while the pressure of the system drops. The pressure drops for two reasons: (i) H_2 consumption to form hydrogen hydrates, and (ii) the temperature decrease leads to pressure drops. To eliminate the effect of temperature on pressure drop, we also conducted a control experiment with an empty chamber (i.e. only H_2 without water and porous material) to subtract this factor from our calculations. This means we only consider pressure drops attributed to hydrate formation. This ensures that our calculations are devoid of temperature-related effects. We also used the control experiment to calculate the cooling rate of the chamber, which was then used to calculate the total heat released from hydrate formation. It is critical to emphasize that both experiments have been conducted in the same setup and immediately after each other, with no changes to the setup other than adding the sample. This approach minimizes error by ensuring identical conditions for both control and actual experiments. Additionally, each experiment is repeated multiple times to ensure precision and consistency in our results. Pressure and temperature of the system were continuously recorded until no further changes were observed and the system stabilized. After completion of formation, dissociation of hydrogen hydrate was done by increasing the temperature of the system to room temperature, and the release rate of the stored was measured by recording the pressure changes inside the chamber during dissociation. The release process was completed when no further

pressure change was observed inside the chamber.

2. Results and discussion

2.1. Surface chemistry

The chemistry of the pore surface and its interaction with water plays a critical role in hydrate nucleation and hydrogen storage. Here, we took advantage of the Si–*O*–H groups of Z3 to activate ice-like bonds at the interface of mesopores [38]. These bonds are generated through the process of mesoporous generation as discussed below. The ice-like structure through its effect on interfacial energy, *m*, will further enhance the nucleation rate of hydrates. The calculation of m in the shape function is not straightforward, but as the interface of water-Z3 resembles that of the water-ice interface, we expect the value of *m* to approach 1, Supplementary Materials, S4. We characterized chemistry of Z3 material and other zeolite structures to access the ratio of Si/Al in these structures which directly affects the interaction of these materials with water molecules as shown in Supplementary Materials, S5. The chemical analysis by Inductively coupled Plasma-optical (ICP-OES) shows that Z3 has Si/Al ratio of 16.09 which is an order of magnitude higher than other zeolite structures. The introduction of mesopores by application of the alkaline surfactant treatment has also introduced Si–OH groups on the external surface of Z3. In the next step, we analyzed the zeolite Y before and after treatment to access the activation of Si–*O*–H bonds on Z3 surfaces through FTIR spectroscopy as shown in Fig. 2a. Typically, O–H stretches of terminal silanol groups, Si–*O*–H, and strong Bronsted acid sites, Si–O (-H)-Al, in zeolite Y are observed at 3740 cm^{-1} and 3620 cm^{-1}, respectively. As expected, after the generation of mesopores in zeolite Y, silanol defects lead to an increase in the intensity of the Si–*O*–H peak at 3740 cm^{-1}. Similarly, the defects generated caused some loss of Al from the zeolite framework as evident from the decrease in intensity of the Si–O (-H)-Al peak at 3620 cm^{-1}. It is worth noting that the starting zeolite Y was in its proton (H^+) form, and NH_4OH was used as the base to create the high pH environment required for the generation of mesopores. Thus, zeolite Y remained in its H+ form, even after the treatment.

We examined the bonding type of water molecules in the bulk solution of water/THF and water/THF confined in pores of Z3 through FTIR spectroscopy (Fig. 2b and **c**). We observed that water confined in Z3 pores shows enhanced DDAA bonds compared to DA bonds, suggesting the formation of ice-like structures in the confined water. For the Z3 material, the ratio of DDAA to DA bonds is 1.57, while this ratio is 0.94 for bulk water. We conducted FTIR spectroscopy for commercial zeolites with other pore sizes and for mesoporous carbon as shown in Supplementary Materials, S6. For all materials examined, we did not observe an enhanced effect of DDAA to DA ratio comparable to that of Z3. For zeolites with 4 and 10 nm pores, this ratio drops to 1.25 and

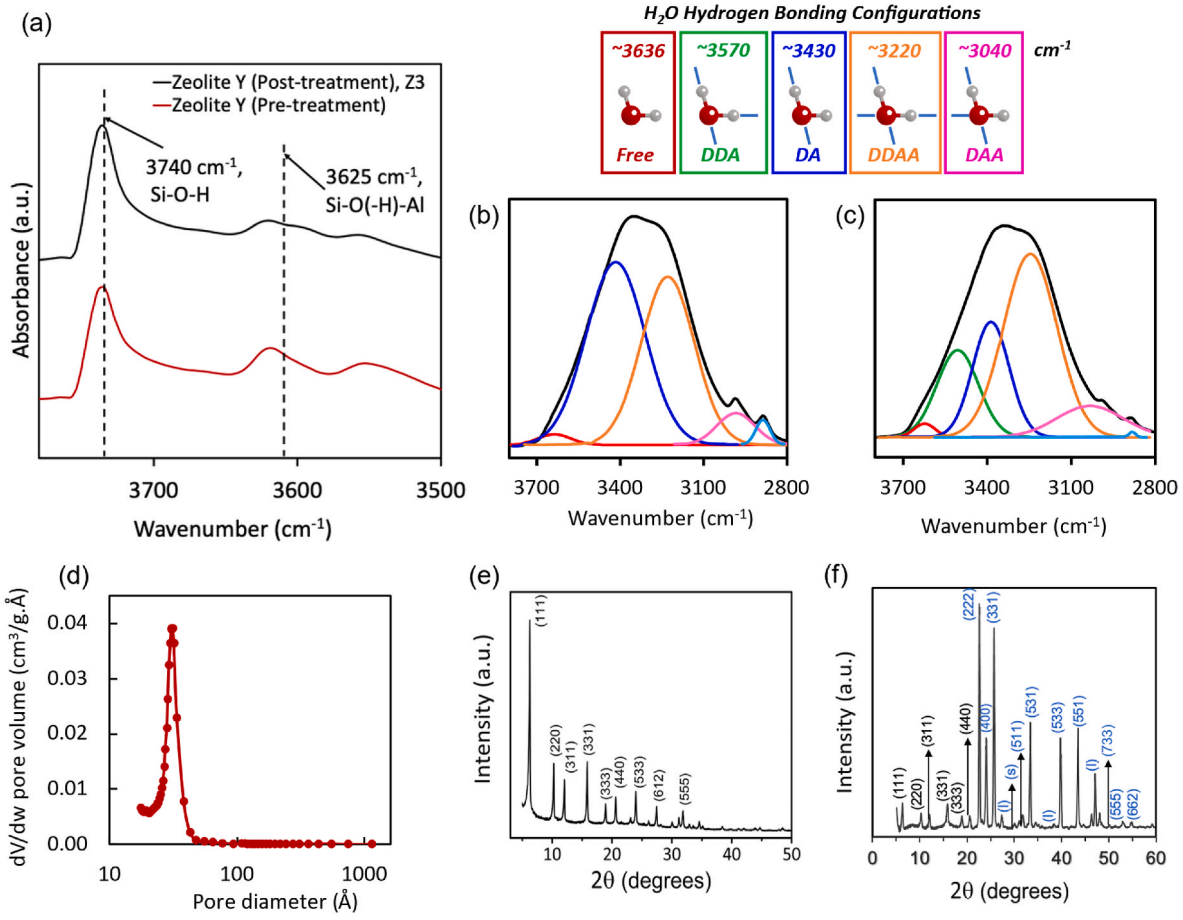

Fig. 2. **(a)** Enhancement of Si–*O*–H bonds at the surface of Z3 to activate ice-like bonding with water molecules**, (b)** Bonding nature of water molecules probed by FTIR spectroscopy for bulk water and THF and **(c)** Z3 filled with water and THF solution. Black curve corresponds to the experimental data. Compared to the bulk material, Z3 has fewer DA bonds and more DDAA bonds indicating the formation of ice-like structures at the water-pore wall interface. The ratio of DDAA to DA bonds is 1.57 for Z3 compared to 0.94 for bulk water. **(d)** Pore Size Distribution (PSD) of Z3 determined via BET test. The PSD profile confirms the presence of narrow mesopores, around 2 nm. **(e)** Powder X-ray diffraction pattern of Z3 confirming the zeolite FAU crystal structure without any detectable impurities. **(f)** X-ray diffraction pattern of Z3/hydrogen hydrate confirming the presence of hydrogen hydrate. The black labels refer to Z3 and blue labels refer to hydrogen hydrate [43]. (For interpretation of the references to colour in this figure legend, the reader is referred to the Web version of this article.)

1.21, respectively. For mesoporous carbon, the ratio shows a much lower value of 1.10. Fig. 2d shows a narrow distribution of pore sizes in Z3 and thus confirms the uniformity of the pore dimensions in Z3. Furthermore, we conducted X-ray diffraction of Z3 to confirm its crystallinity (FAU framework type), Fig. 2e. Overall, the optimal pore size and specific surface chemistry of Z3 enables a decrease in the Gibb's energy barrier for hydrogen hydrates to nucleate at much lower pressures than in bulk systems.

2.2. Hydrogen storage

We used the developed material framework of Z3, approximately 5 g for each experiment, for hydrogen storage through hydrogen hydrates. The experimental platform and procedure are discussed in Supplementary Materials, S7. The closed system includes water, 10 mol% THF promoter, the material framework, and H_2 gas. In the system, the material framework is placed at the bottom of the chamber, and the chamber is filled with hydrogen gas to initiate hydrogen storage. As shown in Fig. 3a, the hydrate formation occurs in two distinct steps: (i) hydrogen diffusion in water and (ii) hydrate nucleation and growth. These two steps are separated by an induction period. This period is characterized by the time to attain stable hydrate nuclei that can grow continuously into bulk hydrate crystals. As hydrogen gas diffuses in the water or hydrate phase nucleates, the pressure in the chamber drops. This behavior resembles quasi-isobaric conditions at ~10 bar since the pressure change is less than 0.5 bar. The pressure variation in the hydrate formation process within Z3 is shown in Fig. 3a. Within 10 min, we observe that the water confined in the pores is fully saturated with hydrogen gas and no further hydrogen can dissolve in the water. That is, a large volume of Z3 could be saturated with water quickly. In contrast, for bulk water, based on the diffusion coefficient of hydrogen gas in water (4.5×10^{-5} $cm^{-2}s^{-1}$) and considering bulk water as a semi-infinite medium, hydrogen molecules could only diffuse within 300 μm length of bulk water in 10 min phase suggesting that hydrate formation in bulk water is limited to a thin layer and scale up process is a challenge.

After the induction period, the hydrate phase nucleates at the pore wall-water interface as it is characterized by a drop in hydrogen pressure and a release of heat as indicated by an enthalpic increase in the liquid-solid phase (an exothermic process). We probed the temperature of the system as a function of time for the Z3 sample, as shown in Fig. 3b. To perform X-ray diffraction (XRD) analysis, the sample is carefully transfer into the XRD instrument under low-temperature conditions using a dry-ice environment. This precaution is taken to ensure that the sample remains cool and does not experience any heat-related effects. It has been indicated that simple H_2O–H_2 clathrates begin to release hydrogen as the temperature increases [39–41]. Accordingly, our XRD investigation was carried out at a temperature of 190K and atmospheric pressure, as depicted in Fig. 2f. A XRD analysis of the H_2/THF hydrate clearly indicates the presence of a sII hydrate crystal structure, which is in agreement with previous studies by Florusse et al. [46]. However, we observed slight differences in peak intensities between our XRD pattern and the reported XRD pattern. These discrepancies can be attributed to the distinct environmental conditions under which hydrogen hydrate formation occurs. Specifically, the reported data pertains to bulk hydrogen hydrate, while our hydrogen hydrate is formed within a confined environment. In despite these minor differences, there is overall agreement in the sII hydrate crystal structure based on similarities in XRD patterns of hydrogen hydrate in bulk and confined hydrogen hydrate. We emphasize that control experiments were conducted before each experiment to accurately capture the kinetics of hydrate formation. In addition to sample Z3, we probed hydrogen hydrate formation in mesoporous zeolite 13X (FAU type) with pores 4 nm and 10 nm in the course of our work. Through integration of the temperature-time curves, we determined the heat released in the system through hydrate formation, **Supplementary Information, S8**. This information along with the enthalpy of phase change allows the determination of hydrogen hydrate formation for each material framework. Having the amount of hydrogen stored through pressure drop curves (Fig. 3a) and the mass of the formed hydrogen hydrate, we determined the hydrogen storage capacity of Z3 and zeolites with other pore sizes (Fig. 4a).

At a pressure of ~10 bar, Z3 possess a hydrogen storage capacity of hydrate at 2.1 wt%, which is approaching the maximum storage capacity of cubic hydrogen hydrate structure II for a solution of water and 10 mol% THF (i.e., ~2.1 wt%) [27]. The storage capacity of 5.1 wt% can be achieved for pure water but requires a much higher pressure of approximately 200 MPa [42]. As we limited the operating pressure range between 4 and 12 bar in this work, we did not examine hydrogen hydrate formation in pure water. In the context of volumetric storage capacity, Z3 possess a hydrogen storage capacity of 0.00274 kg/L at 10 bar. The storage capacity of the system is determined by considering the total mass of the system. As shown Fig. 4c, Z3 exhibits storage capacities of 0.33 %, 0.45 %, and 0.55 % at of 6, 8, and 10 bar, respectively. The raw data for Z3 at pressures of 6, 8, and 10 bar are shown in Figs. S9–S11. For zeolite 13X with 4 nm pore size, the hydrogen storage capacity of hydrate is 1.9 wt% at 10 bar. The raw data for zeolite 13X with 4 nm pores at pressures of 6, 8, and 10 bar are shown in Figs. S11–S13. In zeolite 13X with 10 nm pore size, we could not form hydrogen hydrate up to a pressure of 10 bar, but approaching 12 bar, we achieved a hydrogen storage capacity of hydrate of 1.1 wt%. The raw data for zeolite 13X with 10 nm pores at pressures of 12 and 10 bar are shown in Figs. S15–S16. We emphasize that we could not form hydrogen hydrates in zeolite 13X with 10 nm and 10 bar (or other lower pressures). In addition, the raw data for mesoporous carbon at 11 bar (Fig. S17) indicate no hydrogen hydrate formation. Fig. S18 shows the freezing temperature of water/THF within the Z3 in the absence of

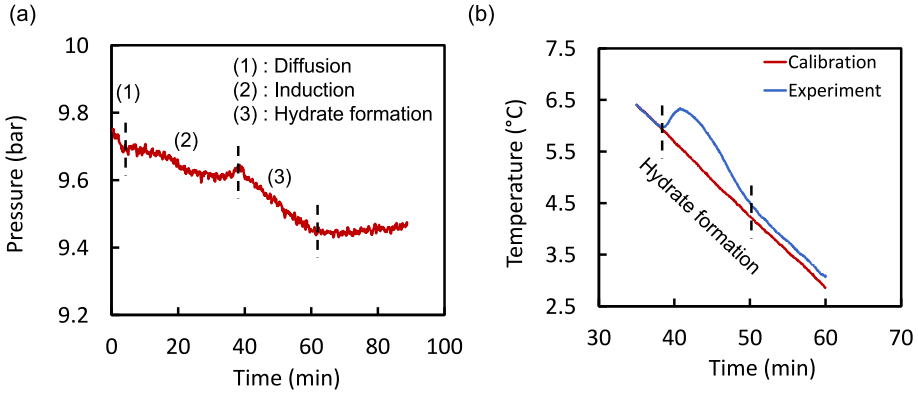

Fig. 3. (a) Temporal pressure of the system during hydrate formation in sample Z3 at 10 bar, which is approximated as a quasi-isobaric process. **(b)** Temporal temperature of the system during hydrate formation in sample Z3 at 10 bar.

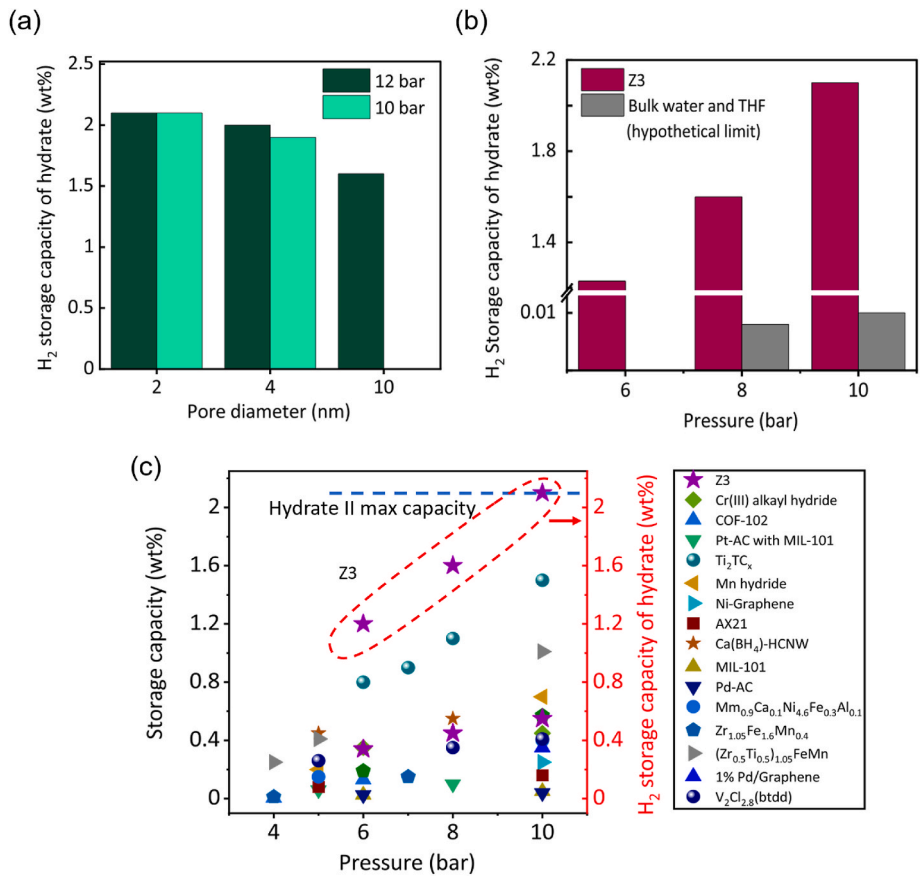

Fig. 4. **(a)** Hydrogen storage capacity of hydrates with various pore dimensions are compared with Z3 offering 2.1 % storage capacity, which is the maximum capacity of the cubic hydrogen hydrate structure for 10 mol % THF solution. **(b)** Hydrogen storage capacity of Z3 vs bulk water and THF are shown [44], which suggest that storage capacity can be boosted by more than 200 times by Z3 structures. **(c)** Storage capacity of Z3 is compared with other state-of-the-art material in the pressure range of 4–10 bar.

hydrogen. This experimental procedure was carried out under two distinct conditions: under atmospheric pressure and under argon pressure similar to our main hydrogen-inclusive experiment. This investigation aimed to study the freezing point of water/THF within the Z3 sample. This finding suggests that hydrogen solubility at few nanometer pores play a critical role for hydrate formation at these low operating pressures. To emphasize the dramatic role of restructuring water molecules in confined spaces and DDAA water bonds for hydrate formation, we compared the hydrogen storage capacity of Z3 with bulk water at various pressures (Fig. 4b). The effect of restructuring water and tuning the bonding nature of the water-pore wall enhanced the storage capacity by more than two orders of magnitude. We should emphasize that we conducted the hydrogen storage experiments with mesoporous carbon of 1.8 nm pore diameter as a control, but no hydrate formation could be measured; therefore, it is apparent that the combination of optimal pore size and surface chemistry is required to achieve this unprecedented hydrogen storage capacity.

Fig. 4c compares the hydrogen storage capacity of Z3 with other state-of-the-art materials in the operating pressure range of 4–12 bar. We chose this pressure range based on system feasibility for onboard light-duty vehicles and portable power applications. We note further that we limited the temperature range of storage materials to −40 to 85 °C based on the DOE target for 2025. Under these ranges of operating conditions, Z3 offers modest storage capacity compared to the state-of-the-art materials and promises a disruptive platform for hydrogen storage technologies. In addition to high storage capacity, Z3 has other advantages on charging/discharging rates compared to the state-of-the-art materials as discussed below.

The hydrogen charging rate plays an important role in the implementation of hydrogen storage technologies. The charging times of various state-of-the-art materials are shown in Fig. 5a. The charging pressure for each material is depicted on each graph. Despite having the lowest charging pressure and highest storage capacity, Z3 surprisingly exhibits the shortest charging time compared to other materials. For most of the materials, the discharging of hydrogen is achieved through high temperatures or under vacuum conditions, which significantly limits the deployment of these structures in various applications. The discharging time of various hydrogen storage materials along with their corresponding discharging temperature is provided in Fig. 5b. For some of these materials, temperatures approaching 700 K are required for H_2 discharging. The mesoporous zeolite Z3 has one of the lowest discharging times at ambient discharging temperature. These performance criteria demonstrate the many advantages and potential utility that Z3 offers as a H_2 storage material.

3. Conclusion

Hydrogen storage systems are crucial to the successful transition to sustainable energy and offer strategies to address climate challenges. High storage capacity at moderate pressure and temperature, fast charging and discharging along with low-cost and safety are the principal merits of these systems. In this study, we introduced a new material to store hydrogen in the molecular structure of water with no deleterious environmental effects. The components for this storage method are water, THF and modified Zeolite out of which water and THF are commodity and modified Zeolite could be synthesized through a well-established synthesis process suggesting potential of Z3 to be scaled-up and be implemented in large stationary or compact mobile settings.

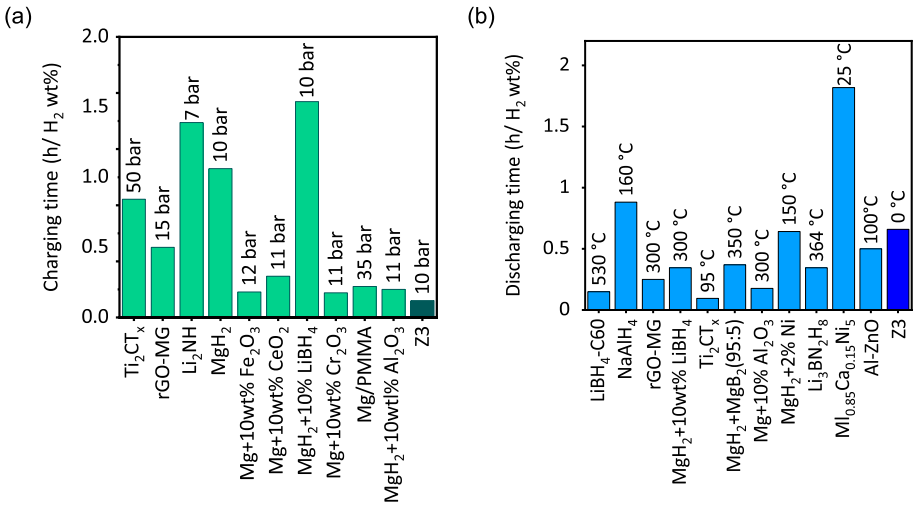

Fig. 5. (a) Hydrogen charging times of various material storage media are compared, and their corresponding pressures are labeled on each bar. **(b)** Hydrogen discharging times of various materials are compared. For some materials, the temperatures in the range of 750 K are required for H_2 discharge. Sample Z3 provides ambient temperature discharging with short discharging times. The combined fast charging and discharging times with minimal energy makes Z3 a superior material for hydrogen storage [20,45-59].

We envision that the localized interfacial and confined hydrogen storage described here will enable safe hydrogen deployment in a broad spectrum of energy systems from power generation to land and ocean transportation.

Associated content

Online content

The Supporting Information is available online (Microsoft document).

Contributions

H.G. conceived the idea. A.A. synthesized the materials with guidance by J.D.R. and T.R.L. R.F. and A. A. conducted the main experiments and A.H., S.N. and Z.H. helped on the experiments. R.F. and H.G. wrote the manuscript with inputs from all the authors. All authors commented on the manuscript. H. G. directed the research.

Declaration of competing interest

The authors declare the following financial interests/personal relationships which may be considered as potential competing interests: Hadi Ghasemi reports financial support was provided by ACS Petroleum Research Fund. Hadi Ghasemi reports financial support was provided by Office of Naval Research. Hadi Ghasemi reports financial support was provided by Center of Carbon Management in Energy. Jeffrey Rimer reports financial support was provided by Welch Foundation. T. Randall Lee reports financial support was provided by US Air Force Office of Scientific Research. T. Randall Lee reports financial support was provided by Robert A. Welch Foundation. Hadi Ghasemi has patent pending to University of Houston.

Data availability

Data will be made available on request.

Acknowledgement

We acknowledge the funding support by ACS Petroleum Research Fund (Grant No. 59590) with Burtrand Lee as the program manager, Office of Naval Research (Grant No. N00014-23-1-2034) with Dr. Mark Spector as the program manager and Center of Carbon Management in Energy (CCME) at University of Houston. J.D.R. acknowledges funding from the Welch Foundation (Grant No. E-1794). T.R.L. acknowledges support from the US Air Force Office of Scientific Research (FA9550-20-1-0349; 20RT0302) and the Robert A. Welch Foundation (Grant No. E-1320).

Appendix A. Supplementary data

Supplementary data to this article can be found online at https://doi.org/10.1016/j.mtphys.2023.101248.

References

[1] H. Ritchie, M. Roser, Energy. *Our World in Data*, 2020.
[2] B.J. van Ruijven, E. De Cian, Sue Wing, I. Amplification of future energy demand growth due to climate change, Nat. Commun. 10 (2019) 1–12.
[3] J. Tollefson, Hydrogen vehicles: fuel of the future? Nature 464 (2010) 1262–1264, https://doi.org/10.1038/4641262a. Preprint at.
[4] E.J. Griffith, Hydrogen fuel, Nature 248 (1974) 458.
[5] H. Council, Hydrogen Scaling up, 2017.
[6] M. Jacoby, Filling up with hydrogen, Chem. Eng. News 83 (2005) 42–47, https://doi.org/10.1021/cen-v083n034.p042. Preprint at.
[7] P. Jena, Materials for hydrogen storage: past, present, and future, J. Phys. Chem. Lett. 2 (2011) 206–211, https://doi.org/10.1021/jz1015372. Preprint at.
[8] T.S. Blankenship, N. Balahmar, R. Mokaya, Oxygen-rich microporous carbons with exceptional hydrogen storage capacity, Nat. Commun. 8 (2017) 1–12.
[9] P.M. Forster, et al., Adsorption of molecular hydrogen on coordinatively unsaturated Ni(II) sites in a nanoporous hybrid material, J. Am. Chem. Soc. 128 (2006) 16846–16850.
[10] E.S. Cho, et al., Graphene oxide/metal nanocrystal multilaminates as the atomic limit for safe and selective hydrogen storage, Nat. Commun. 7 (2016) 1–8.
[11] W. Jiang, Y. Chen, X. Mo, X. Li, First-principles investigation of LaMg2Ni and its hydrides, Sci. Rep. 10 (2020) 1–11.
[12] E. Mamontov, A.I. Kolesnikov, S. Sampath, J.L. Yarger, Hydrogen mobility in the lightest reversible metal hydride, LiBeH3, Sci. Rep. 7 (2017) 1–7.
[13] H. Nishino, et al., Formation and characterization of hydrogen boride sheets derived from MgB2 by cation exchange, J. Am. Chem. Soc. 139 (2017) 13761–13769.
[14] Q. Hu, et al., A new family of promising hydrogen storage medium, J. Phys. Chem. A 117 (2013) 14253–14260.
[15] G. Li, et al., Hydrogen storage in Pd nanocrystals covered with a metal-organic framework, Nat. Mater. 13 (2014) 802–806.
[16] S. Liu, et al., Hydrogen storage in incompletely etched multilayer Ti2CTx at room temperature, Nat. Nanotechnol. 16 (2021) 331–336.
[17] Y. Li, R.T. Yang, Hydrogen storage in low silica type X zeolites, J. Phys. Chem. B 110 (2006) 17175–17181.
[18] E.M. Borzone, A. Baruj, M.V. Blanco, G.O. Meyer, Dynamic measurements of hydrogen reaction with LaNi5-xSn x alloys, Int. J. Hydrogen Energy 38 (2013) 7335–7343.

[19] M.S. Choudhari, V.K. Sharma, M. Paswan, Metal hydrides for thermochemical energy storage applications, Int. J. Energy Res. 45 (2021) 14465–14492, https://doi.org/10.1002/er.6818. Preprint at.
[20] S. Liu, et al., Hydrogen storage in incompletely etched multilayer Ti2CTx at room temperature, Nat. Nanotechnol. 16 (2021) 331–336.
[21] J. Farrando-Perez, et al., Rapid and efficient hydrogen clathrate hydrate formation in confined nanospace, Nat. Commun. 13 (2022) 5953.
[22] P. Di Profio, S. Arca, F. Rossi, M. Filipponi, Comparison of hydrogen hydrates with existing hydrogen storage technologies: energetic and economic evaluations, Int. J. Hydrogen Energy 34 (2009) 9173–9180.
[23] L.N. Ho, Y. Schuurman, D. Farrusseng, B. Coasne, Solubility of gases in water confined in nanoporous materials: ZSM-5, MCM-41, and MIL-100, J. Phys. Chem. C 119 (2015) 21547–21554.
[24] H. Lee, et al., Tuning clathrate hydrates for hydrogen storage, Nature 434 (2005) 743–746.
[25] Hydrogen Storage | Department of Energy.
[26] W.L. Vos, L.W. Finger, R.J. Hemley, H. Mao, Novel H2-H2O clathrates at high pressures, Phys. Rev. Lett. 71 (1993) 3150–3153.
[27] R.K. Zhdanov, et al., Phase diagram and composition of water based crystalline phases in hydrogen – water binary system, Solid State Commun. 294 (2019) 6–10.
[28] R.G. Grim, et al., Synthesis and characterization of sI clathrate hydrates containing hydrogen, J. Phys. Chem. C 116 (2012) 18557–18563.
[29] T.A. Strobel, C.A. Koh, E.D. Sloan, Water cavities of sH clathrate hydrate stabilized by molecular hydrogen, J. Phys. Chem. B 112 (2008) 1885–1887.
[30] G.R. Qian, A.O. Lyakhov, Q. Zhu, A.R. Oganov, X. Dong, Novel hydrogen hydrate structures under pressure, Sci. Rep. 4 (2014) 1–5.
[31] A. Davoodabadi, A. Mahmoudi, H. Ghasemi, The potential of hydrogen hydrate as a future hydrogen storage medium, iScience 24 (2021): 101907.
[32] T.J. Frankcombe, G.J. Kroes, Molecular dynamics simulations of type-sII hydrogen clathrate hydrate close to equilibrium conditions, J. Phys. Chem. C 111 (2007) 13044–13052.
[33] J. García-Martínez, M. Johnson, J. Valla, K. Li, J.Y. Ying, Mesostructured zeolite Y—high hydrothermal stability and superior FCC catalytic performance, Catal. Sci. Technol. 2 (2012) 987.
[34] A. Chawla, N. Linares, J.D. Rimer, J. García-Martínez, Time-resolved dynamics of intracrystalline mesoporosity generation in USY zeolite, Chem. Mater. 31 (2019) 5005–5013.
[35] B. Coasne, D. Farrusseng, Gas oversolubility in nanoconfined liquids: review and perspectives for adsorbent design, Microporous Mesoporous Mater. 288 (2019): 109561.
[36] L.N. Ho, Y. Schuurman, D. Farrusseng, B. Coasne, Solubility of gases in water confined in nanoporous materials: ZSM-5, MCM-41, and MIL-100, J. Phys. Chem. C 119 (2015) 21547–21554.
[37] A. Hakimian, et al., Freezing of few nanometers water droplets, Nat. Commun. 12 (2021) 6973.
[38] D.T. Bregante, et al., The shape of water in zeolites and its impact on epoxidation catalysis, Nat. Catal. 4 (2021) 797–808.
[39] N.I. Papadimitriou, I.N. Tsimpanogiannis, A.T. Papaioannou, A.K. Stubos, Evaluation of the hydrogen-storage capacity of pure H2 and binary H2-THF hydrates with Monte Carlo simulations, J. Phys. Chem. C 112 (2008) 10294–10302.
[40] T.A. Strobel, et al., Molecular hydrogen storage in binary THF-H2 clathrate hydrates, J. Phys. Chem. B 110 (2006) 17121–17125.
[41] A. Giannasi, M. Celli, L. Ulivi, M. Zoppi, Low temperature Raman spectra of hydrogen in simple and binary clathrate hydrates, J. Chem. Phys. 129 (2008).
[42] J. Farrando-Perez, et al., Rapid and efficient hydrogen clathrate hydrate formation in confined nanospace, Nat. Commun. 13 (2022).
[43] A.J. Heinrich, J.A. Gupta, C.P. Lutz, D.M. Eigler, Single-atom spin-flip spectroscopy, Science 306 (2004) 466–469, 1979.
[44] N.I. Papadimitriou, I.N. Tsimpanogiannis, A.T. Papaioannou, A.K. Stubos, Evaluation of the hydrogen-storage capacity of pure H2 and binary H2-THF hydrates with Monte Carlo simulations, J. Phys. Chem. C 112 (2008) 10294–10302.
[45] V. Stavila, R.K. Bhakta, T.M. Alam, E.H. Majzoub, M.D. Allendorf, Reversible hydrogen storage by NaAlH4 confined within a titanium-functionalized MOF-74 (Mg) nanoreactor, ACS Nano 6 (2012) 9807–9817.
[46] E.S. Cho, et al., Graphene oxide/metal nanocrystal multilaminates as the atomic limit for safe and selective hydrogen storage, Nat. Commun. 7 (2016).
[47] H. Lee, et al., Tuning clathrate hydrates for hydrogen storage, Nature 434 (2005) 743–746.
[48] K.J. Jeon, et al., Air-stable magnesium nanocomposites provide rapid and high-capacity hydrogen storage without using heavy-metal catalysts, Nat. Mater. 10 (2011) 286–290.
[49] M. Song, J.-L. Bobet, B. Darriet, Improvement in hydrogen sorption properties of Mg by reactive mechanical grinding with Cr2O3, Al2O3 and CeO2, J. Alloys Compd. 340 (2002) 256–262.
[50] J.W. Prendergast, Hydrogen Desorption and Absorption for Activated Magnesium Hydride, University of Birmingham, 2010.
[51] Y.H. Hu, E. Ruckenstein, Hydrogen storage of Li 2NH prepared by reacting Li with NH 3, Ind. Eng. Chem. Res. 45 (2006) 182–186.
[52] Y. Chen, C. Wu, P. Wang, H. Cheng, Structure and hydrogen storage property of ball-milled LiNH2/MgH2LiNH2/MgH2 mixture, Int. J. Hydrogen Energy 31 (2006) 1236–1240.
[53] P.A. Ward, et al., Reversible hydrogen storage in a LiBH4-C60 nanocomposite, J. Phys. Chem. C 117 (2013) 22569–22575.
[54] Y. Chen, C. Sequeira, C. Chen, X. Wang, Q. Wang, Metal hydride beds and hydrogen supply tanks as minitype PEMFC hydrogen sources, Int. J. Hydrogen Energy 28 (2003) 329–333.
[55] X.B. Yu, D.M. Granty, G.S. Walker, Low-temperature dehydrogenation of LiBH4 through destabilization with TiO2, J. Phys. Chem. C 112 (2008) 11059–11062.
[56] M. Ahmad, Rafi-Ud-din, C. Pan, J. Zhu, Investigation of hydrogen storage capabilities of ZnO-based nanostructures, J. Phys. Chem. C 114 (2010) 2560–2565.
[57] N.I. Papadimitriou, I.N. Tsimpanogiannis, C.J. Peters, A.T. Papaioannou, A. K. Stubos, Hydrogen storage in sH hydrates: a Monte Carlo study, J. Phys. Chem. B 112 (2008) 14206–14211.
[58] T. Hügle, M.F. Kühnel, D. Lentz, Hydrazine borane: a promising hydrogen storage material, J. Am. Chem. Soc. 131 (2009) 7444–7446.
[59] R. Gosalawit-Utke, et al., LiF-MgB2 system for reversible hydrogen storage, J. Phys. Chem. C 114 (2010) 10291–10296.